



Ferrum-molybdenum dual incorporated cobalt oxides as efficient bifunctional anti-corrosion electrocatalyst for seawater splitting

Wenxian Liu ^a, Wenbin Que ^a, Ruilian Yin ^b, Jiale Dai ^a, Dong Zheng ^a, Jinxiu Feng ^a, Xilian Xu ^a, Fangfang Wu ^a, Wenhui Shi ^c, Xijun Liu ^d, Xiehong Cao ^{a,*}

^a College of Materials Science and Engineering, Zhejiang University of Technology, Hangzhou 310014, PR China

^b College of Chemical Engineering, Zhejiang University of Technology, Hangzhou 310014, PR China

^c Center for Membrane Separation and Water Science & Technology, Zhejiang University of Technology, Hangzhou 310014, PR China

^d School of Resource, Environments and Materials, Guangxi University, Nanning 530004, PR China



ARTICLE INFO

Keywords:

Seawater splitting
Electrocatalysis
Hydrogen generation
Nanosheet assembly
Chemical doping

ABSTRACT

Electrochemical seawater splitting is a potentially attractive technology for sustainable hydrogen production; however, its implementation is severely hindered by the lack of active and anti-corrosion catalysts. Here, a monolithic Fe-Mo-Co-O nanosheet assembly is reported, comprising Fe-doped $\text{Co}_2\text{Mo}_3\text{O}_8/\text{MoO}_3/\text{Co}_3\text{O}_4$ hybridized nanosheets decorated on nickel foam (FMCO/NF). The intelligent combination of corrosion-resistant Mo-O species and highly active Fe dopant afford FMCO/NF with high activity and durability for water splitting in both freshwater, simulated seawater, and real seawater media. Specifically, the symmetric FMCO/NF-based alkaline electrolyzer generates 10 mA cm^{-2} at a low voltage of 1.58 V, outperforming the benchmark $\text{IrO}_2/\text{NF}||\text{Pt/C}/\text{NF}$ and many non-noble metal-based catalysts. Moreover, an alkaline seawater electrolyzer with low cell voltage, good durability, and high Faradaic efficiency was manufactured by using monolithic FMCO/NF as both cathode and anode. This work offers a new path toward the design of highly efficient and anti-corrosion catalysts for hydrogen generation from seawater.

1. Introduction

Hydrogen (H_2) with high energy density (142 MJ kg^{-1}) and pollution-free features is regarded as a promising alternative to traditional fossil fuels. [1–3] Electrochemical water electrolysis, comprising hydrogen evolution reaction (HER) at cathode and oxygen evolution reaction (OER) at anode, offers a sustainable and efficient route for H_2 production. [4–6] In the past decade, many efficient water electrolyzers have been developed based on freshwater electrolytes, which put a heavy strain on scarce freshwater resources. Electrolysis of seawater, which accounts for ~ 96.5% of the global water, becomes a promising alternative for large-scale H_2 production. [7,8] However, the implementation of seawater splitting technologies remains extremely challenging, due to the sluggish OER and HER kinetics, undesirable chlorine oxidation reaction (ClOR), and the corrosion of electrodes caused by the aggressive salts in seawater. [9,10].

Transition metal oxides particularly Co_3O_4 are considered as promising candidates for various electrocatalytic processes, owing to their reasonable stability, high environmental compatibility, and electronic

state/chemical composition flexibility. [11–14] Based on the Sabatier principle, the adsorption energy of intermediates (e.g., $^*\text{OH}$ and $^*\text{OOH}$ for OER, and $^*\text{H}$ for HER) should be at the optimum value. Specifically, too-strong bindings may poison the surface and disrupt the subsequent catalytic cycle, and too-weak bindings will result in ineffective adsorption thus limiting the overall activity. [15–17] Unfortunately, inherent scaling relation results in that the adsorption energies of reaction intermediates (e.g., OOH^* and OH^*) on a single catalytic site cannot be optimized independently, thereby delivering unsatisfactory catalytic activity. [18,19] Recent theoretical calculations and experimental results demonstrate that a small amount of Fe doping into Co_3O_4 can optimize the energetics of the OER intermediates to enhance the intrinsic catalytic activity. [20,21] On the other hand, integrating multiple active sites into one material is an effective way to endow materials with multifunctional catalytic activities. For instance, Yu et al. constructed a bimetallic electrocatalyst comprising Co-Mo dual sites and discovered that the Co site was responsible for O-H bond cleavage in H_2O and the Mo center undertook hydrogen evolution. [17] Ren et al. reported a Ni-Fe bimetallic oxy-hydroxide exhibited satisfactory OER

* Corresponding author.

E-mail address: gescaoxh@zjut.edu.cn (X. Cao).

activity in both alkaline simulated seawater (1 M KOH + 0.5 M NaCl) and alkaline natural seawater (1 M KOH + seawater) electrolytes, respectively. [22] In addition, $\text{Co}_3\text{O}_4\text{-Mo}_2\text{N}$, $\text{Co}_3\text{O}_4\text{-Ni}_2\text{P}$, and $\text{Co}_3\text{O}_4\text{-Mo}_3\text{O}_3$ were demonstrated to have much better OER/HER activity and water splitting performance than the pristine Co_3O_4 . [23–25] Nevertheless, the introduction of suitable dopant into multi-site Co_3O_4 -based catalysts for efficient seawater splitting has rarely been reported.

Another major challenge associated with seawater splitting is the existence of aggressive Cl^- , which results in electrode corrosion and undesirable chlorine oxidation. [26–28] Several routes have been explored to address these problems, including in-situ coating of cation-selective polyanions, and decorating chloride-retarding components (e.g., CeO_x , CaCO_3 , and Cr(OH)_3) on the electrode. [7,29,30] Very recently, Chen et al. utilized pre-adsorbed SO_4^{2-} to repel Cl^- to achieve improved stability of the NiFe-layered double hydroxide (NiFe-LDH) in alkaline seawater electrolysis. [31] Unfortunately, the introduction of inert anti-corrosion layers would possibly compromise electrocatalytic activity due to blocked active sites and unfavorable mass transfer. [30, 32] The introduction of corrosion-resistant components without sacrificing activity is of great significance but rarely achieved. Thus, it is extremely demanded but challenging to manufacture highly efficient and robust bifunctional multimetallic electrodes with high anti-corrosion property for H_2 production from real seawater splitting.

Herein, we report an assembly of Fe-doped $\text{Co}_2\text{Mo}_3\text{O}_8/\text{MoO}_3/\text{Co}_3\text{O}_4$ hybridized nanosheets decorated on nickel foam (denoted as FMCO/NF) that exhibits impressive activity and durability for water splitting in both freshwater, simulated seawater, and real seawater media. Molybdenum oxides were demonstrated to have good corrosion resistance due to they can transform into MoO_4^{2-} that provides ion selectivity to repel aggressive Cl^- . [33–35] The introduction of Mo-O species on the one hand improves the corrosion resistance of the FMCO/NF electrode, [36] and on the other hand, serves as optimized active sites for OER and HER along with Fe dopant. Simultaneously, the unique nanosheet assembly structure enables accelerated mass transfer and highly exposed active sites. Consequently, the FMCO/NF electrode exhibits outstanding OER and HER activities, and enables an efficient alkaline electrolyzer with a low cell voltage of 1.58 V at a current density of 10 mA cm^{-2} , outperforming many non-noble metal-based catalysts. More importantly, a seawater electrolyzer was successfully constructed using FMCO/NF as both cathode and anode, which requires only 1.59 V to achieve 10 mA cm^{-2} , and shows impressive stability along with high Faradaic efficiency of about 98.1%.

2. Experimental section

2.1. Synthesis of Co-2-methylimidazole/Ni foam (Co-mim/NF)

Co-mim was synthesized according to previous works. [37] Typically, 0.5821 g 2-methylimidazole was dissolved in 40 mL H_2O . Afterwards, the above solution was added to an aqueous solution (40 mL) of $\text{Co}(\text{NO}_3)_2\cdot 6 \text{ H}_2\text{O}$ (1.3 g) and stirred for 2 min. The pre-treated Ni foam (NF, 2 cm × 2.5 cm) was soaked into the mixed solution for 4 h at room temperature. After the reaction, Co-mim/NF was washed with deionized water and placed in a vacuum oven at 60 °C for 12 h.

2.2. Synthesis of FeMoCo-mim/NF and FMCO/NF

Typically, 0.0648 g $\text{Na}_2\text{MoO}_4\cdot 2 \text{ H}_2\text{O}$ and 0.0135 g $\text{Fe}(\text{NO}_3)_3\cdot 9 \text{ H}_2\text{O}$ ($\text{Mo:Fe} = 8:1$) was dissolved in a mixture of 14.4 mL N,N -dimethylformamide (DMF) and 0.6 mL H_2O . Then, the above solution and a piece of precursor (Co-mim/NF) were sealed in a 50 mL Teflon-lined autoclave and maintained at 150 °C for 6 h. After cooling to room temperature, the as-synthesized yellow FeMoCo-mim/NF was washed with DMF and methanol three times, and then dried at 60 °C for 12 h. Subsequently, the prepared FeMoCo-mim/NF was placed in a tubular furnace, and annealed at 280 °C with a heating rate of 10 °C min^{-1} in Ar/H_2 (volume ratio = 9:1) for 1 h, followed by another annealing at 450 °C for 2 h to obtain FMCO/NF.

2.3. Synthesis of $\text{Co}_3\text{O}_4/\text{NF}$ and $\text{MoO}_3/\text{Co}_3\text{O}_4/\text{NF}$

$\text{Co}_3\text{O}_4/\text{NF}$ was synthesized as follows: The as-synthesized Co-mim/NF was firstly placed in a tubular furnace, and annealed at 700 °C with a heating rate of 10 °C min^{-1} in N_2 for 2 h, then heated at 450 °C in the air for 30 min. The $\text{MoO}_3/\text{Co}_3\text{O}_4/\text{NF}$ was obtained by mixing 1.0 mg of commercial MoO_3 and a piece of $\text{Co}_3\text{O}_4/\text{NF}$ (1 cm × 1 cm, containing approximately 0.92 mg Co_3O_4).

2.4. Material characterization

X-ray diffraction (XRD) patterns were recorded with a PANalytical X'Pert PRO powder diffractometer using $\text{Cu K}\alpha$ radiation ($\lambda = 0.1541 \text{ nm}$). The microstructures and compositions of the samples were measured by field emission scanning electron microscopy (FESEM, FEI Nova NanoSEM 450) and transmission electron microscopy (TEM, FEI Talos S-FEG) equipped with an EDS detector. X-ray photoelectron spectroscopy (XPS) was performed on a Shimadzu Kratos Axis Ultra-DLD. Raman spectra were collected on a Horiba Jobin Yvon LabRAM HR800 with a 532 nm laser. The element contents of the samples were

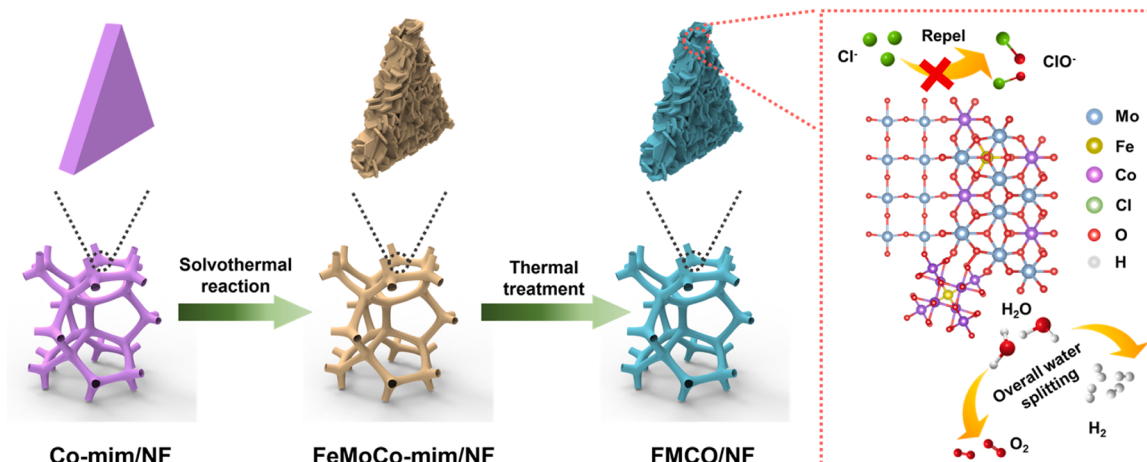


Fig. 1. Schematic illustration of the preparation route of the FMCO/NF catalysts.

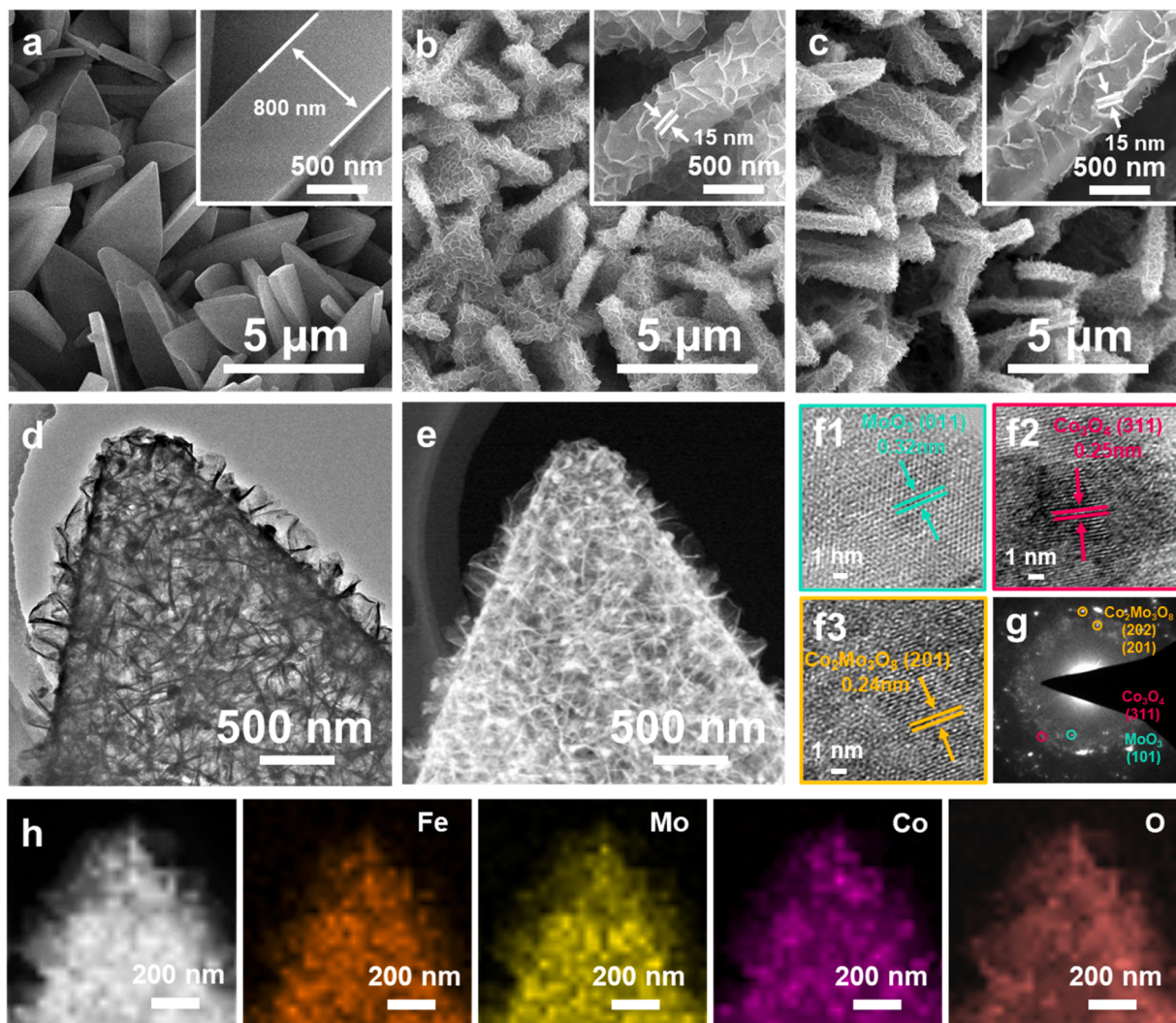


Fig. 2. (a) SEM images of Co-mim/NF. (b) SEM images of FeMoCo-mim/NF. (c-h) Characterizations of FMCO/NF: (c) SEM images, (d) TEM image, (e) HAADF-STEM image, (f1-f3) HRTEM images, (g) SAED pattern, and (h) EDS elemental mapping images.

detected by inductively coupled plasma-optical emission spectrometry (ICP-OES, Agilent 720ES).

2.5. Electrochemical measurements

All electrochemical measurements were performed on CHI 760e (CH Instruments, Inc., Shanghai, China). The seawater used in this work comes from the Ningbo Zhoushan Port of China, and the main components are Na^+ (12994 ppm), Mg^{2+} (1598 ppm), Ca^{2+} (563 ppm), Cl^- (26428 ppm). Oxygen evolution reaction (OER) and hydrogen evolution reaction (HER) were conducted in three-electrode system, and overall freshwater/seawater splitting test was performed in a two-electrode system. A graphite rod was applied as a counter electrode, and a saturated calomel electrode (SCE) was used as a reference electrode. The prepared FMCO/NF was directly used as the working electrodes. Catalyst inks of Pt/C (20%), IrO_2 , and MoO_3 were fabricated by mixing 5 mg catalyst, 32 μL Nafion in a mixture of 768 μL deionized water and 200 μL ethanol, then coating on NF with the loading of 1 mg cm^{-2} .

Linear sweep voltammetry (LSV) polarization curves were obtained at a slow scan rate of 5 mV s^{-1} with 90% iR compensation unless otherwise specified. Three different electrolytes, including 1 M KOH, 1 M KOH + 0.5 M NaCl, and 1 M KOH + seawater, were used, and the pH was around 14. Electrochemical impedance spectroscopy (EIS) was carried out in the frequency range from 0.01 to 100000 Hz at open

circuit potential in 1 M KOH electrolyte. All potentials in this work were calibrated to the reversible hydrogen electrode (RHE) according to the following equation: $E_{\text{RHE}} = E_{\text{SCE}} + 0.241 + 0.059 \times \text{pH}$. Corrosion potential and corrosion current of FMCO/NF were obtained from polarization tests in seawater electrolyte. The overall water-splitting system was performed using FMCO/NF as both anode and cathode in a two-electrode configuration. The electrochemically active surface area (ECSA) was estimated by the double-layer capacitance, which was calculated based on the cyclic voltammograms (CV) collected between 10 and 50 mV s^{-1} in the non-Faradaic potential region in 1 M KOH. [38] The ECSA was calculated according to the following equation: $\text{ECSA} = C_{\text{dl}}/C_s$, where C_{dl} is the electrochemical double layer capacitance and C_s represent the specific capacitance (0.040 mF cm^{-2}). [39].

3. Results and discussion

3.1. Morphological and structural analysis

The fabrication procedure of FMCO/NF assembly is illustrated in Fig. 1. Co-2-methylimidazole (Co-mim) framework nanosheets were first deposited on the NF substrate through a facile solution method. Then, the as-prepared Co-mim/NF was employed as a sacrificial template to react with additional ferric ion and molybdate to form a 2D/3D FeMoCo-mim nanosheet assembly via a possible dissolution-

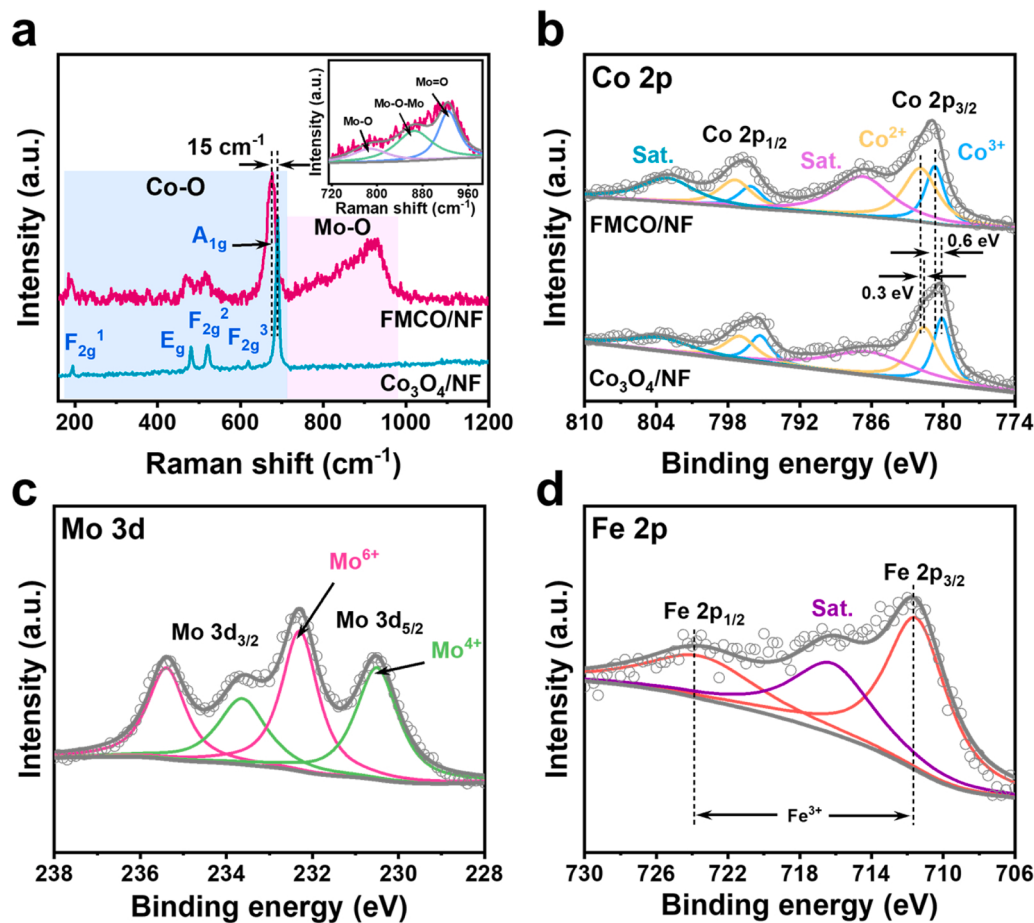


Fig. 3. (a) Raman spectra of FMCO/NF and Co₃O₄/NF. (b-d) High-resolution XPS spectra of FMCO/NF and Co₃O₄/NF: (b) Co 2p, (c) Mo 3d and (d) Fe 2p.

recrystallization process. [38,40,41] Finally, after thermal treatment in Ar/H₂ (volume ratio = 9:1) atmosphere, hierarchical Fe-doped Co₂Mo₃O₈/MoO₃/Co₃O₄ (FMCO) hybridized nanosheets were formed on NF substrate. The in-situ pyrolysis of FeMoCo-mim framework guarantees the tight contact among each component in FMCO, which not only enhances the stability of the hybrid but also promotes the electronic interaction between multiple active sites. Moreover, the incorporation of Mo species can further optimize the adsorption of HER/OER intermediates, as well as improve corrosion resistance properties (Fig. S1). [42,43] All of these ingenious designs make FMCO/NF as a promising electrocatalyst for seawater splitting.

Scanning electron microscopy (SEM) images in Fig. 2a show that smooth-surfaced Co-mim nanosheets with thickness of ~ 800 nm evenly cover on the NF surface. After reacting with Fe(NO₃)₃ and Na₂MoO₄ in a mixture of N,N-dimethylformamide (DMF) and H₂O, the 2D sheet-like skeleton was maintained and many interconnected nanoflakes with thickness of about 15 nm appear on their surfaces (Fig. 2b). The phase transformation of Co-mim was further confirmed by X-ray diffraction (XRD), as evidenced by the disappearance of Co-mim characteristic peaks (Fig. S2a). Energy dispersive X-ray spectroscopy (EDS) results in Fig. S2b reveal the successful introduction of Fe and Mo elements in FeMoCo-mim. Fig. 2c and the inset show the SEM images of the FMCO/NF. One can see that the nanosheet-assembled hierarchical structure was well preserved during the pyrolysis process. Transmission electron microscopy (TEM) and high-angle annular dark-field scanning TEM (HAADF-STEM) images in Fig. 2d, e further confirm that numerous nanoflakes are attached to the sheet-like scaffold, forming a hierarchical architecture. Fig. 2f display high-resolution TEM (HRTEM) images of FMCO scraped from NF, showing lattice fringes with inter-planar distance of 0.33, 0.25, and

0.24 nm, which can be assigned to the (011) plane of MoO₃, (311) plane of Co₃O₄, and (201) plane of Co₂Mo₃O₈, respectively. The selected area electron diffraction (SAED) pattern in Fig. 2g further confirms the coexistence of MoO₃, Co₃O₄, and Co₂Mo₃O₈ in the FMCO. EDS elemental mapping images (Fig. 2h) clearly show that Fe, Mo, Co, and O elements are uniformly distributed throughout the whole FMCO assembly. Additionally, the inductively coupled plasma-optical emission spectrometry (ICP-OES) analysis indicates that the molar ratio of Fe:Mo:Co is 1:4.7:10 in the FMCO hybrid.

XRD, Raman, and X-ray photoelectron spectroscopy (XPS) measurements were carried out to analyze the structural and chemical characteristics of the FMCO/NF. XRD pattern (Fig. S3) confirm the presence of crystalline Co₂Mo₃O₈ (JCPDS No. 71-1423), MoO₃ (JCPDS No. 85-2405), and Co₃O₄ (JCPDS No. 80-1536) in FMCO/NF. It is noteworthy that no peaks of Fe-based compounds were detected in the XRD pattern, implying that Fe species are present as dopant. From the Raman spectra in Fig. 3a, both the FMCO/NF and Co₃O₄/NF (Fig. S1c, d) exhibits F_{2g}¹, E_g, F_{2g}², F_{2g}³, and A_{1g} characteristic peaks of Co₃O₄ in the region of 180–720 cm⁻¹. Further observation shows that the A_{1g} peak of FMCO/NF is located at ~ 675 cm⁻¹, which is 15 cm⁻¹ lower than that of the Co₃O₄/NF. This red-shift phenomenon further verifies the doping of Fe in FMCO/NF. [44,45] In addition, the Raman spectrum of FMCO/NF (inset of Fig. 3a) shows three deconvoluted peaks at 786, 864, and 926 cm⁻¹, assigning to the stretching mode of Mo-O, Mo-O-Mo, and Mo=O bands, respectively. [46–48] Fig. 3b shows high-resolution XPS spectra of Co 2p for FMCO/NF and Co₃O₄/NF. The pristine Co₃O₄/NF exhibits two pairs (2p_{3/2}/2p_{1/2}) of peaks at 780.1/785.3 eV and 781.6/797.0 eV, corresponding to Co³⁺ and Co²⁺, respectively. [49,50] After the incorporation of Fe-Mo species, the binding energy of both Co³⁺ and Co²⁺ increases, implying that the Co sites in FMCO/NF are

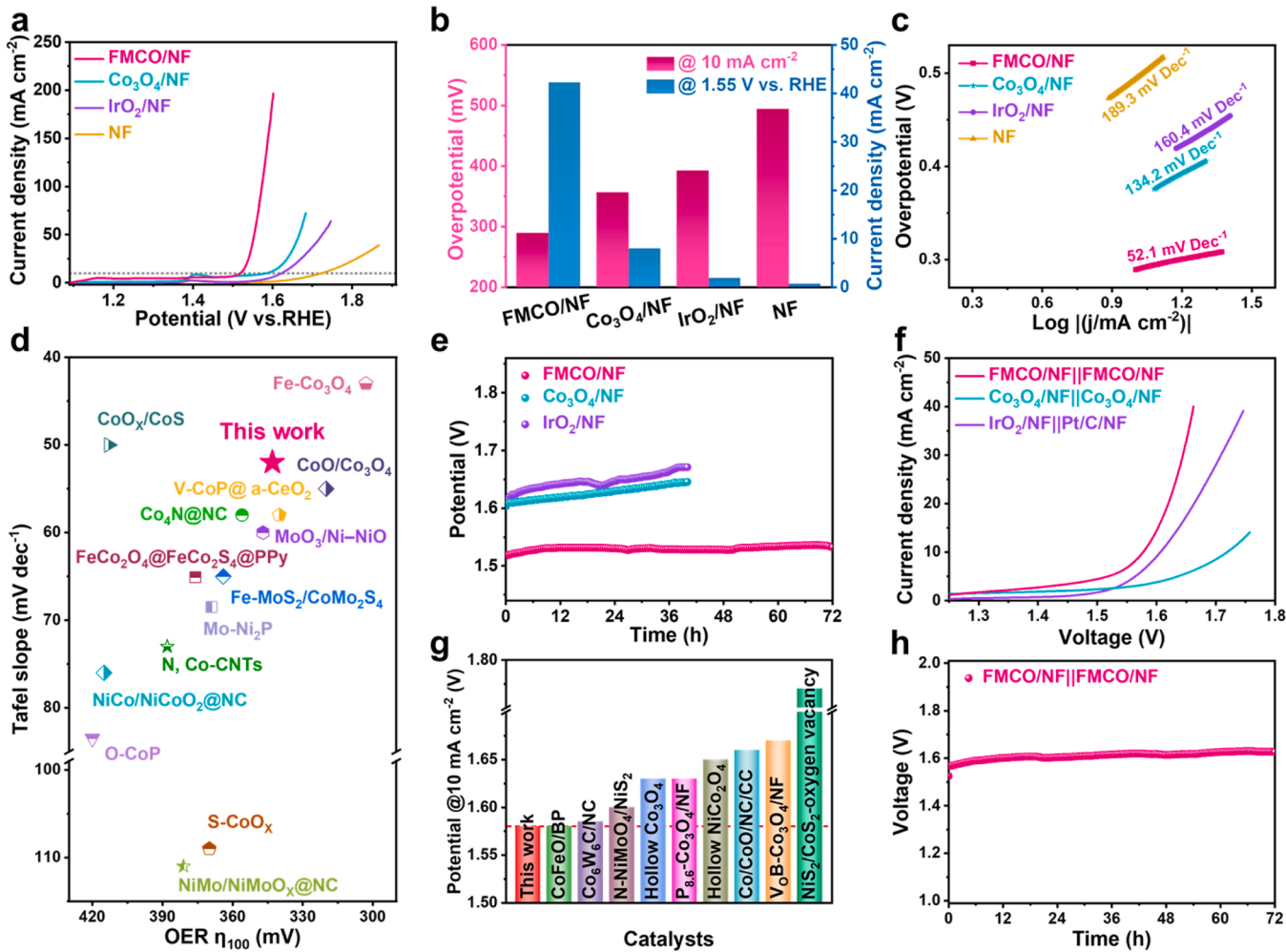


Fig. 4. (a) OER polarization curves for FMCO/NF, $\text{Co}_3\text{O}_4/\text{NF}$, IrO_2/NF and NF electrodes in 1 M KOH. (b) Comparison of overpotentials at 10 mA cm^{-2} (red histogram) and current density at 1.55 V (vs. RHE, blue histogram) for the prepared catalysts. (c) Tafel plots of various prepared catalysts. (d) Comparison of the overpotentials for OER (at 100 mA cm^{-2}) and Tafel plots of the prepared FMCO/NF and other reported electrocatalysts. (e) Electrochemical stability of the FMCO/NF, $\text{Co}_3\text{O}_4/\text{NF}$ and IrO_2/NF electrodes. (f) Polarization curves of the prepared FMCO/NF and other catalysts for overall water splitting in 1 M KOH. (g) Comparison of cell voltage of the catalysts at the current density of 10 mA cm^{-2} . (h) Stability of the FMCO/NF||FMCO/NF electrolyzer in 1 M KOH at 10 mA cm^{-2} .

more positively charged, which can facilitate the adsorption of anionic intermediates in OER for the fast redox process thus lead to accelerated catalytic kinetics. [51,52] The deconvoluted Mo 3d spectrum (Fig. 3c) of FMCO/NF displays four peaks at 230.5, 232.3, 233.6, and 235.4 eV, which can be assigned to Mo^{4+} 3d_{5/2}, Mo^{6+} 3d_{5/2}, Mo^{4+} 3d_{3/2}, and Mo^{6+} 3d_{3/2}. [53,54] The O 1 s XPS spectrum of FMCO/NF (Fig. S4) exhibits three peaks at 530.2, 530.7, and 531.5 eV, corresponding to Co-O, Mo-O, and adsorbed O, respectively. [55,56] The Fe 2p peaks in FMCO/NF are located at 711.5 and 723.5 eV, revealing Fe exists in the +3 oxidation state (Fig. 3d). [57,58] Previous experimental and theoretical calculation results show that Fe^{3+} doping can optimize the binding energy of reaction intermediates (e.g., OH^*) at active sites and enhance the catalytic activity. [59,60].

3.2. OER/HER and overall water splitting performance in alkaline freshwater electrolyte

The OER and HER activities of FMCO/NF were first evaluated in 1.0 M KOH freshwater electrolyte by directly using the self-supported monolithic catalyst as the working electrode. Fig. 4a shows the OER polarization curve of FMCO/NF compared with that of $\text{Co}_3\text{O}_4/\text{NF}$, IrO_2/NF , and bare NF. Obviously, the FMCO/NF exhibits the best OER activity with an overpotential of 289 mV to afford a current density of

10 mA cm^{-2} , significantly lower than those for the $\text{Co}_3\text{O}_4/\text{NF}$ (356 mV), IrO_2/NF (392 mV), and NF (494 mV). Moreover, the FMCO/NF delivers a current density of 41.9 mA cm^{-2} at 1.55 V (vs. RHE), which is 5.3, 24.6, and 69.8 times those of $\text{Co}_3\text{O}_4/\text{NF}$, IrO_2/NF , and NF (Fig. 4b). Notably, OER and HER activities of FMCO/NF is much higher than other comparison samples, including MoO_3/NF , $\text{Co}_3\text{O}_4/\text{MoO}_3/\text{NF}$, $\text{Co}_2\text{Mo}_3\text{O}_8/\text{NF}$, and Fe-doped $\text{Co}_3\text{O}_4/\text{NF}$, due to the synergistic effect between each component (Fig. S5-S10). The electrochemical active surface area (ECSA) normalized polarization curves (Fig. S11) further reveal the highest intrinsic OER activity of FMCO/NF, compared to the control samples. As shown in Fig. 4c, the FMCO/NF exhibits the lowest Tafel slope of 52.1 mV dec^{-1} in comparison with that of $\text{Co}_3\text{O}_4/\text{NF}$ ($134.2 \text{ mV dec}^{-1}$), IrO_2/NF ($160.4 \text{ mV dec}^{-1}$), and NF ($189.3 \text{ mV dec}^{-1}$), indicating more favorable OER kinetics on the FMCO/NF. In addition, electrochemical impedance spectroscopy (EIS) of the samples was conducted to further investigate the reaction kinetics. Fig. S12 clearly reveals the smallest charge transfer resistance (R_{ct}) of FMCO/NF, confirming its fast charge transfer. Notably, the OER activity and Tafel slope of FMCO/NF were comparable and even superior to those of recently reported non-noble metal-based OER electrocatalysts (Fig. 4d and Table S1). Chronopotentiometry tests show the satisfactory stability of FMCO/NF at current densities of 10 mA cm^{-2} over 72 h, while the operating potential of $\text{Co}_3\text{O}_4/\text{NF}$ and IrO_2/NF suffered an obvious

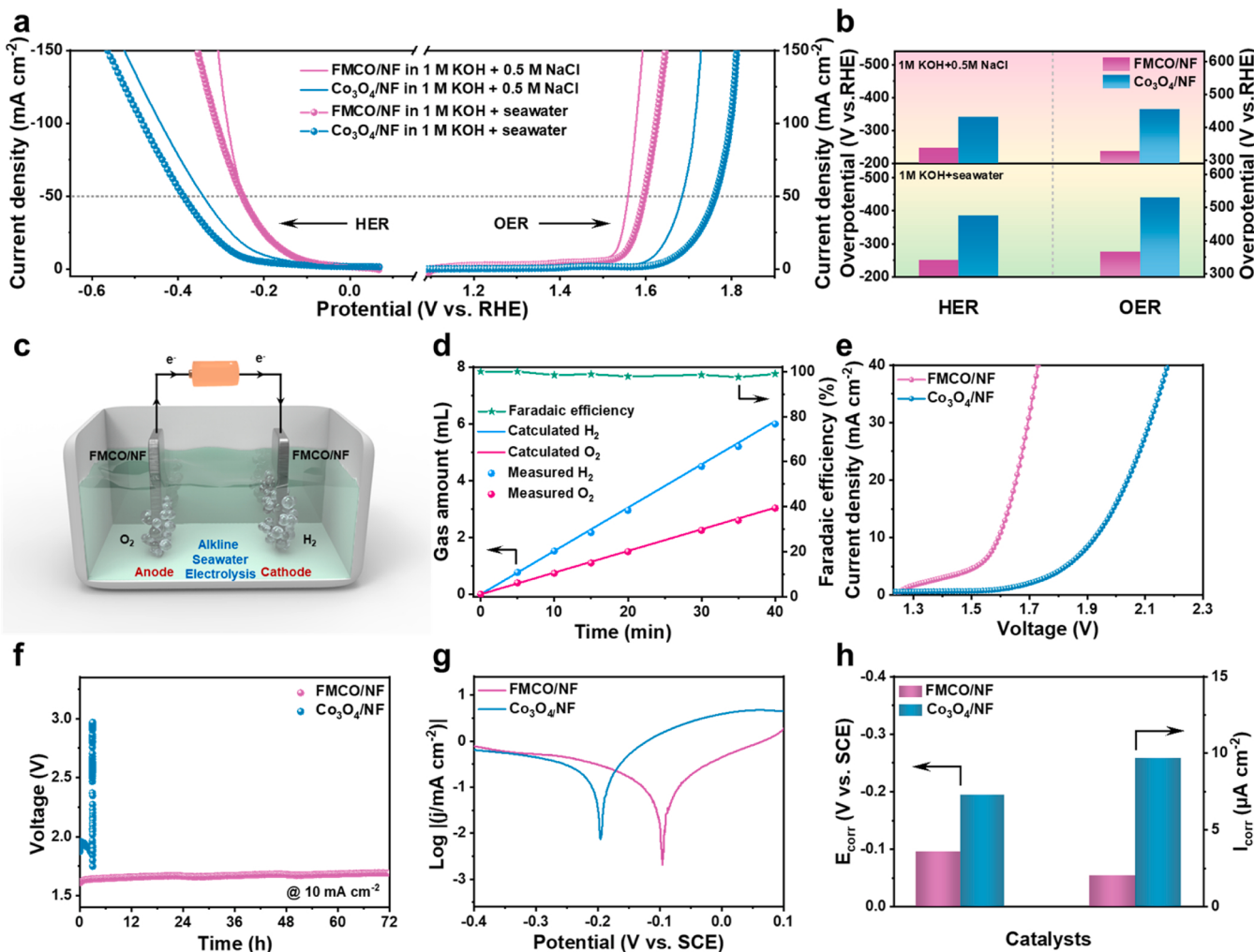


Fig. 5. (a) OER and HER polarization curves for FMCO/NF and Co₃O₄/NF electrodes in 1 M KOH + 0.5 M NaCl and 1 M KOH + seawater, respectively. (b) Comparison of HER and OER overpotentials at 50 mA cm⁻² for FMCO/NF and Co₃O₄/NF catalysts in 1 M KOH + 0.5 M NaCl and 1 M KOH + seawater, respectively. (c) Schematic diagram for overall seawater splitting by FMCO/NF||FMCO/NF. (d) Faradaic efficiency of FMCO/NF for water splitting in 1 M KOH + 0.5 M NaCl. (e) Polarization curves of FMCO/NF||FMCO/NF and Co₃O₄/NF||Co₃O₄/NF electrolyzers in 1 M KOH + seawater electrolyte. (f) Stability of the FMCO/NF||FMCO/NF and Co₃O₄/NF||Co₃O₄/NF electrolyzer in alkaline seawater electrolyte at 10 mA cm⁻². (g) Tafel polarization curves of different samples in natural seawater. (h) Comparison of E_{corr} and I_{corr} on FMCO/NF and Co₃O₄/NF catalysts.

increase within 40 h (Fig. 4e). Impressively, the FMCO/NF exhibits high HER capability with overpotential of 87 mV at 10 mA cm⁻² and Tafel slope of 147.1 mV dec⁻¹ in 1 M KOH, lower than 181 mV and 154.5 mV dec⁻¹ of Co₃O₄/NF (Fig. S13). Inspired by superior OER and HER performance, the monolithic FMCO/NF was assembled as both anode and cathode in a two-electrode.

alkaline electrolyzer. The polarization curves show that FMCO/NF||FMCO/NF electrolyzer requires a low voltage of 1.58 V to afford a current density of 10 mA cm⁻², suppressing Co₃O₄/NF||Co₃O₄/NF (1.72 V), the benchmark IrO₂/NF||Pt/C/NF (1.61 V), and many recent reports such as CoFeO/BP, Co₆W₆C/NC, Ni-NiMoO₄/NiS₂, hollow Co₃O₄, P_{8.6}-Co₃O₄, hollow NiCo₂O₄, etc (Fig. 4f, g and Table S2). Moreover, the FMCO/NF electrode maintain the excellent activity after 72 h continuous water splitting test at 10 mA cm⁻² (Fig. 4 h). Thus, the incorporation of Fe-Mo species makes FMCO/NF a highly active and robust electrocatalyst for OER, HER and overall water splitting in alkaline freshwater media.

3.3. Overall seawater splitting performance and anti-corrosion properties

Further, the OER and HER performance of FMCO/NF in alkaline simulated seawater electrolyte (1 M KOH + 0.5 M NaCl) and alkaline

natural seawater electrolyte (1 M KOH + seawater) were investigated (Fig. 5a, b). As can be observed, the FMCO/NF requires low overpotentials of 328 and 248 mV for OER and HER at 50 mA cm⁻² in 1 M KOH + 0.5 M NaCl, respectively, outperforming those of 454 and 342 mV for the Co₃O₄/NF. In 1 M KOH + seawater electrolyte, OER and HER activities of Co₃O₄/NF exhibits significantly decay, which might be caused by the poisoning of microbes and small particulates in natural seawater. [22,61] As a contrast, the FMCO/NF shows a small attenuation and exhibits low overpotentials of 365 and 250 mV for OER and HER at 50 mA cm⁻², respectively. The long-term stability of FMCO/NF electrode for HER and OER was tested at 100 mA cm⁻² in 1 M KOH + seawater electrolyte for 180 h (Fig. S14 and S15). As shown in Fig. S14a-b and S15a-b, the FMCO/NF exhibits nearly constant operating potentials at the current density of 100 mA cm⁻² in 1 M KOH + seawater electrolyte for 180 h (about 12 mV increase for HER and 33 mV increase for OER), demonstrating satisfactory stability. Remarkably, the 3D nanosheet assembly structure and crystalline structure of FMCO/NF are maintained after 180 h of HER (Fig. S14c-d) and OER (Fig. S15c-d) test. The appearance of Co(OH)₂, change of Co³⁺/Co²⁺ and Mo⁶⁺/Mo⁴⁺ ratio may be attributed to surface reconstruction of catalysts during HER and OER in 1 M KOH + seawater electrolyte (Fig. S14e-h and S15e-h), which is consistent with previous

reports. [62,63] As shown in Fig. S16, a peak at 819 cm^{-1} ascribed to MoO_4^{2-} appeared in the Raman spectrum of FMCO/NF after OER in 1 M KOH + seawater for 24 h, indicating the formation of MoO_4^{2-} during the catalytic process which can provide ion selectivity to repel aggressive Cl^- . [33,64,65] Encouraged by the high OER and HER activities of FMCO/NF, we set up an overall seawater splitting device in alkaline seawater electrolytes, in which the monolithic FMCO/NF was used as both anode and cathode (Fig. 5c). Remarkably, the FMCO/NF-based electrolyzer requires a low cell voltage of 1.58 V to afford current density of 10 mA cm^{-2} in 1 M KOH + 0.5 M NaCl electrolyte, superior to 1.94 V of $\text{Co}_3\text{O}_4/\text{NF}$ (Fig. S17). The generated gaseous products on the cathode and anode over the H-type electrolyzer in 1 M KOH + 0.5 M NaCl electrolyte was collected to evaluate the Faradaic efficiency (Fig. S18). As shown in Fig. 5d, the volume ratio of H_2 and O_2 released from the cathode and anode is close to 2:1, and the Faradaic efficiency is calculated to be as high as 98.1%, demonstrating high selectivity towards the OER. N, N-diethyl-phenylenediamine (DPD) method was used to detect whether the chlorine evolution reaction occurred during the overall seawater splitting process. As shown in Fig. S19, no discoloration in the 1 M KOH + seawater electrolyte after 72 h of stability test at the current density of 240 mA cm^{-2} can be observed, indicating no hypochlorite and/or hypochlorous acid formation. The FMCO/NF = | FMCO/NF electrolyzer produces a low cell voltage of 1.59 V at 10 mA cm^{-2} , 1.97 V at 240 mA cm^{-2} , and long-term stability over 72 h in 1 M KOH + seawater electrolyte (Figs. 5e, 5f, and S20). As shown in Fig. S21 and S22, the FMCO/NF = | FMCO/NF electrolyzer exhibit excellent stability over 180 h in 1 M KOH + seawater (Fig. S21) and 450 h in 30 wt% KOH + 0.5 M NaCl electrolyte at 240 mA cm^{-2} (Fig. S22), which provides a promising way for H_2 production from seawater electrolysis. It is worth noting that the stability of FMCO/NF = | FMCO/NF seawater splitting electrolyzer is comparable to or even better than many recently reported symmetric and asymmetric electrolyzers (Table S3).

Tafel extrapolation measurement was conducted in natural seawater to further verify the anti-corrosion performance of FMCO/NF, and the Tafel plots and related corrosion parameters were presented in Fig. 5g,h. Corrosion potential and corrosion current are important parameters that connect the practical corrosion behavior of electrodes. Generally, a higher corrosion potential reflects a lower tendency for corrosion and a lower corrosion current indicates a lower corrosion rate. [27,66] Obviously, FMCO/NF has a higher corrosion potential (-0.096 V vs. SCE) and lower corrosion current ($2.04\text{ }\mu\text{A cm}^{-2}$) than those of $\text{Co}_3\text{O}_4/\text{NF}$ (-0.194 V and $9.67\text{ }\mu\text{A cm}^{-2}$). These results suggest that the rationally designed FMCO/NF electrode has a higher anti-corrosion ability than $\text{Co}_3\text{O}_4/\text{NF}$, which is consistent with the result of alkaline seawater electrolysis stability test in Fig. 5f.

4. Conclusions

In summary, a 3D Fe-Mo dual incorporated Co-O nanosheet assembly composed of Fe-doped $\text{Co}_2\text{Mo}_3\text{O}_8/\text{MoO}_3/\text{Co}_3\text{O}_4$ on nickel foam (FMCO/NF) was manufactured as highly efficient and anti-corrosion bifunctional electrocatalyst for seawater splitting. Benefiting from optimized electronic/coordination structure of Fe-doped multimetallic oxide hybrids, high corrosion resistance of Mo-O components, as well as abundant accessible active sites of the 3D nanosheet assembled structure, the fabricated FMCO/NF monolithic electrode exhibits outstanding OER and HER performances in both alkaline freshwater, simulated seawater, and real seawater media. Notably, the FMCO/NF||FMCO/NF electrolyzer in 1.0 M KOH generates 10 mA cm^{-2} at a low voltage of 1.58 V, suppressing $\text{IrO}_2/\text{NF}||\text{Pt/C/NF}$ and many non-noble metal-based catalysts. Furthermore, the FMCO/NF-based alkaline seawater electrolyzer show low potential requirement, high stability, and high Faradaic efficiency of 98.1%. Our work presents a feasible strategy to rationally design multifunctional electrocatalysts with high activity and selectivity.

CRediT authorship contribution statement

Wenxian Liu: Conceptualization, Supervision, Writing - original draft, Writing - review & editing. **Wenbin Que:** Methodology, Data curation, Writing - original draft. **Ruilian Yin:** Data curation, Visualization. **Jiale Dai:** Investigation, Methodology. **Dong Zheng:** Validation, Formal analysis. **Jinxiu Feng:** Data curation, Methodology. **Xilian Xu:** Investigation, Data curation. **Fangfang Wu:** Supervision, Formal analysis. **Wenhui Shi:** Supervision, Methodology. **Xijun Liu:** Methodology, Formal analysis. **Xiehong Cao:** Conceptualization, Funding acquisition, Writing - review & editing.

Declaration of Competing Interest

The authors declare that they have no known competing financial interests or personal relationships that could have appeared to influence the work reported in this paper.

Data availability

Data will be made available on request.

Acknowledgements

This work was supported by the National Natural Science Foundation of China (22275166, 21905246, 51972286, and 22005268), the Zhejiang Provincial Natural Science Foundation of China (LZ21E020003, LR19E020003, LQ21E020004, and LQ20B010011), the Fundamental Research Funds for the Provincial Universities of Zhejiang (RF-B-2020004), National Key Research and Development Project of China (2022YFE0113800).

Appendix A. Supporting information

Supplementary data associated with this article can be found in the online version at doi:10.1016/j.apcatb.2023.122488.

References

- [1] S. Chu, A. Majumdar, Opportunities and challenges for a sustainable energy future, *Nature* 488 (2012) 294–303.
- [2] W. Tong, M. Forster, F. Dionigi, S. Dresp, R. Sadeghi Erami, P. Strasser, A.J. Cowan, P. Farrás, Electrolysis of low-grade and saline surface water, *Nat. Energy* 5 (2020) 367–377.
- [3] F. Sun, J. Qin, Z. Wang, M. Yu, X. Wu, X. Sun, J. Qiu, Energy-saving hydrogen production by chlorine-free hybrid seawater splitting coupling hydrazine degradation, *Nat. Commun.* 12 (2021) 4182.
- [4] L.-G. He, P.-Y. Cheng, C.-C. Cheng, C.-L. Huang, C.-T. Hsieh, S.-Y. Lu, $(\text{Ni}_x\text{Fe}_y\text{Co}_{6-x-y})\text{Mo}_6\text{C}$ cuboids as outstanding bifunctional electrocatalysts for overall water splitting, *Appl. Catal. B Environ.* 290 (2021), 120049.
- [5] A. Li, L. Zhang, F. Wang, L. Zhang, L. Li, H. Chen, Z. Wei, Rational design of porous Ni-Co-Fe ternary metal phosphides nanobricks as bifunctional electrocatalysts for efficient overall water splitting, *Appl. Catal. B Environ.* 310 (2022), 121353.
- [6] C. Wang, M. Zhu, Z. Cao, P. Zhu, Y. Cao, X. Xu, C. Xu, Z. Yin, Heterogeneous bimetallic sulfides based seawater electrolysis towards stable industrial-level large current density, *Appl. Catal. B Environ.* 291 (2021), 120071.
- [7] Y. Kuang, M.J. Kenney, Y. Meng, W.H. Hung, Y. Liu, J.E. Huang, R. Prasanna, P. Li, Y. Li, L. Wang, M.C. Lin, M.D. McGehee, X. Sun, H. Dai, Solar-driven, highly sustained splitting of seawater into hydrogen and oxygen fuels, *Proc. Natl. Acad. Sci. U. S. A.* 116 (2019) 6624–6629.
- [8] S. Dresp, F. Dionigi, M. Klingenhoef, P. Strasser, Direct electrolytic splitting of seawater: opportunities and challenges, *ACS Energy Lett.* 4 (2019) 933–942.
- [9] R.K. Karlsson, A. Cornell, Selectivity between oxygen and chlorine evolution in the chlor-alkali and chlorate processes, *Chem. Rev.* 116 (2016) 2982–3028.
- [10] S. Dresp, T. Ngo Thanh, M. Klingenhoef, S. Brückner, P. Hauke, P. Strasser, Efficient direct seawater electrolyzers using selective alkaline NiFe-LDH as OER catalyst in asymmetric electrolyte feeds, *Energy Environ. Sci.* 13 (2020) 1725–1729.
- [11] Y. Li, X. Wang, J. Miao, J. Li, X. Zhu, R. Chen, Z. Tang, R. Pan, T. He, J. Cheng, Chiral transition metal oxides: synthesis, chiral origins, and perspectives, *Adv. Mater.* 32 (2020), 1905585.
- [12] H. Jung, A. Ma, S.A. Abbas, H.Y. Kim, H.R. Choe, S.Y. Jo, K.M. Nam, A new synthetic approach to cobalt oxides: Designed phase transformation for electrochemical water splitting, *Chem. Eng. J.* 415 (2021), 127958.

[13] H. Liu, Z. Liu, Y. Wang, J. Zhang, Z. Yang, H. Hu, Q. Zhao, H. Ning, L. Zhi, M. Wu, Carbon dots-oriented synthesis of fungus-like CoP microspheres as a bifunctional electrocatalyst for efficient overall water splitting, *Carbon* 182 (2021) 327–334.

[14] X. Zhou, X. Liu, J. Zhang, C. Zhang, S.J. Yoo, J.-G. Kim, X. Chu, C. Song, P. Wang, Z. Zhao, D. Li, W. Zhang, W. Zheng, Highly-dispersed cobalt clusters decorated onto nitrogen-doped carbon nanotubes as multifunctional electrocatalysts for OER, HER and ORR, *Carbon* 166 (2020) 284–290.

[15] Y. Wang, W. Qiu, E. Song, F. Gu, Z. Zheng, X. Zhao, Y. Zhao, J. Liu, W. Zhang, Adsorption-energy-based activity descriptors for electrocatalysts in energy storage applications, *Natl. Sci. Rev.* 5 (2018) 327–341.

[16] D.Y. Kuo, H. Paik, J. Kloppenburg, B. Faeth, K.M. Shen, D.G. Schlam, G. Hautier, J. Suntivich, Measurements of oxygen electroadsorption energies and oxygen evolution reaction on RuO₂(110): a discussion of the sabatier principle and its role in electrocatalysis, *J. Am. Chem. Soc.* 140 (2018) 17597–17605.

[17] K. Zhang, C. Liu, N. Graham, G. Zhang, W. Yu, Modulation of dual centers on cobalt-molybdenum oxides featuring synergistic effect of intermediate activation and radical mediator for electrocatalytic urea splitting, *Nano Energy* 87 (2021), 106217.

[18] Z.-F. Huang, J. Song, S. Dou, X. Li, J. Wang, X. Wang, Strategies to break the scaling relation toward enhanced oxygen electrocatalysis, *Matter* 1 (2019) 1494–1518.

[19] Z.-J. Zhao, S. Liu, S. Zha, D. Cheng, F. Studt, G. Henkelman, J. Gong, Theory-guided design of catalytic materials using scaling relationships and reactivity descriptors, *Nat. Rev. Mater.* 4 (2019) 792–804.

[20] Y. Peng, H. Hajiyani, R. Pentcheva, Influence of Fe and Ni doping on the OER performance at the Co₃O₄(001) surface: Insights from DFT+U calculations, *ACS Catal.* 11 (2021) 5601–5613.

[21] D. Senthil Raja, P.-Y. Cheng, C.-C. Cheng, S.-Q. Chang, C.-L. Huang, S.-Y. Lu, In-situ grown metal-organic framework-derived carbon-coated Fe-doped cobalt oxide nanocomposite on fluorine-doped tin oxide glass for acidic oxygen evolution reaction, *Appl. Catal. B Environ.* 303 (2022), 120899.

[22] L. Yu, L. Wu, B. McElhenny, S. Song, D. Luo, F. Zhang, Y. Yu, S. Chen, Z. Ren, Ultrafast room-temperature synthesis of porous S-doped Ni/Fe (oxy)hydroxide electrodes for oxygen evolution catalysis in seawater splitting, *Energy Environ. Sci.* 13 (2020) 3439–3446.

[23] A. Muthurasu, V. Maruthapandian, H.Y. Kim, Metal-organic framework derived Co₃O₄/MoS₂ heterostructure for efficient bifunctional electrocatalysts for oxygen evolution reaction and hydrogen evolution reaction, *Appl. Catal. B Environ.* 248 (2019) 202–210.

[24] T. Wang, P. Wang, W. Zang, X. Li, D. Chen, Z. Kou, S. Mu, J. Wang, Nanoframes of Co₃O₄-Mo₃N heterointerfaces enable high-performance bifunctionality toward both electrocatalytic HER and OER, *Adv. Funct. Mater.* 32 (2021), 2107382.

[25] C. Zhang, Y. Liu, J. Wang, W. Li, Y. Wang, G. Qin, Z. Lv, A well-designed fencelike Co₃O₄@MoO₃ derived from Co foam for enhanced electrocatalytic HER, *Appl. Surf. Sci.* 595 (2022), 153532.

[26] X. Luo, J. Ji, P. Wang, X. Tan, L. Chen, S. Mu, Spherical Ni₃S₂/Fe-NiP_x magic cube with ultrahigh water/seawater oxidation efficiency, *Adv. Sci.* 9 (2022), 2104846.

[27] S. Liu, S. Ren, R.-T. Gao, X. Liu, L. Wang, Atomically embedded Ag on transition metal hydroxides triggers the lattice oxygen towards sustained seawater electrolysis, *Nano Energy* 98 (2022), 107212.

[28] L. Li, G. Zhang, B. Wang, S. Yang, Constructing the Fe/Cr double (oxy)hydroxides on Fe₃O₄ for boosting the electrochemical oxygen evolution in alkaline seawater and domestic sewage, *Appl. Catal. B Environ.* 302 (2022), 120847.

[29] C. Ros, S. Murcia-Lopez, X. Garcia, M. Rosado, J. Arbiol, J. Llorca, J.R. Morante, Facing seawater splitting challenges by regeneration with Ni-Mo-Fe bifunctional electrocatalyst for hydrogen and oxygen evolution, *ChemSusChem* 14 (2021) 2872–2881.

[30] B. Endrődi, O. Diaz-Morales, U. Mattinen, M. Cuartero, A.K. Padinjarethil, N. Simic, M. Wildlock, G.A. Crespo, A. Cornell, Selective electrochemical hydrogen evolution on cerium oxide protected catalyst surfaces, *Electrochim. Acta* 341 (2020), 136022.

[31] T. Ma, W. Xu, B. Li, X. Chen, J. Zhao, S. Wan, K. Jiang, S. Zhang, Z. Wang, Z. Tian, Z. Lu, L. Chen, The critical role of additive sulfate for stable alkaline seawater oxidation on nickel-based electrodes, *Angew. Chem. Int. Ed.* 60 (2021) 22740–22744.

[32] J.G. Vos, T.A. Wezendonk, A.W. Jeremiassie, M.T.M. Koper, MnO_x/IrO_x as selective oxygen evolution electrocatalyst in acidic chloride solution, *J. Am. Chem. Soc.* 140 (2018) 10270–10281.

[33] J. Li, C. Sun, M. Roostaei, M. Mahmoudi, V. Fattahpour, H. Zeng, J.-L. Luo, Characterization and corrosion behavior of electroless Ni-Mo-P/Ni-P composite coating in CO₂/H₂S/Cl⁻ brine: Effects of Mo addition and heat treatment, *Surf. Coat. Technol.* 403 (2020), 126416.

[34] B. Stalin, G.T. Sudha, C. Kailasanathan, M. Ravichandran, Effect of MoO₃ ceramic oxide reinforcement particulates on the microstructure and corrosion behaviour of Al alloy composites processed by P/M route, *Mater. Today Commun.* 25 (2020), 101655.

[35] M. Chen, Z. Zhang, S. Savilov, G. Wang, Z. Chen, Q. Chen, Enhanced structurally stable cathodes by surface and grain boundary tailoring of Ni-Rich material with molybdenum trioxide, *J. Power Sources* 478 (2020), 229051.

[36] Y. Huang, S. Mu, Q. Guan, J. Du, Corrosion resistance and formation analysis of a molybdate conversion coating prepared by alkaline treatment on aluminum alloy 6063, *J. Electrochem. Soc.* 166 (2019) 224–230.

[37] T. Wang, Z. Kou, S. Mu, J. Liu, D. He, I.S. Amiuin, W. Meng, K. Zhou, Z. Luo, S. Chaemchuen, F. Verpoort, 2D dual-metal zeolitic-imidazolate-framework-(ZIF)-derived bifunctional air electrodes with ultrahigh electrochemical properties for rechargeable zinc-air batteries, *Adv. Funct. Mater.* 28 (2018), 1705048.

[38] Z. Chen, Y. Ha, H. Jia, X. Yan, M. Chen, M. Liu, R. Wu, Oriented transformation of Co-LDH into 2D/3D ZIF-67 to achieve Co-N-C hybrids for efficient overall water splitting, *Adv. Energy Mater.* 9 (2019), 1803918.

[39] L. Wu, L. Yu, F. Zhang, B. McElhenny, D. Luo, A. Karim, S. Chen, Z. Ren, Heterogeneous bimetallic phosphide Ni₂P-Fe₂P as an efficient bifunctional catalyst for water/seawater splitting, *Adv. Funct. Mater.* 31 (2020), 2006484.

[40] Y.T. Xu, Z.M. Ye, J.W. Ye, L.M. Cao, R.K. Huang, J.X. Wu, D.D. Zhou, X.F. Zhang, C. T. He, J.P. Zhang, X.M. Chen, Non-3d metal modulation of a cobalt imidazolate framework for excellent electrocatalytic oxygen evolution in neutral media, *Angew. Chem. Int. Ed.* 58 (2019) 139–143.

[41] P. Hao, H. Wen, Q. Wang, L. Li, Z. Zhao, R. Xu, J. Xie, G. Cui, B. Tang, Superassembly of NiCoO_x solid solution hybrids with a 2D/3D porous polyhedron-on-sheet structure for multi-functional electrocatalytic oxidation, *J. Mater. Chem. A* 9 (2021) 8576–8585.

[42] F. Lin, Z. Dong, Y. Yao, L. Yang, F. Fang, L. Jiao, Electrocatalytic hydrogen evolution of ultrathin Co-Mo₅N₆ heterojunction with interfacial electron redistribution, *Adv. Energy Mater.* 10 (2020), 2002176.

[43] A. Saad, Y. Gao, K.A. Owusu, W. Liu, Y. Wu, A. Ramiere, H. Guo, P. Tsikarais, X. Cai, Ternary Mo₂NiB₂ as a superior bifunctional electrocatalyst for overall water splitting, *Small* 18 (2022), 2104303.

[44] Y. Lu, W. Zhan, Y. He, Y. Wang, X. Kong, Q. Kuang, Z. Xie, L. Zheng, MOF-templated synthesis of porous Co₃O₄ concave nanocubes with high specific surface area and their gas sensing properties, *ACS Appl. Mater. Inter.* 6 (2014) 4186–4195.

[45] Y. Li, K. Li, Y. Wang, K. Zhou, M. Zhao, M. Hu, Y.-Q. Liu, L. Qin, B. Cui, Fe-doped porous Co₃O₄ nanosheets with highly efficient catalytic performance for soot oxidation, *Chem. Eng. J.* 431 (2022), 133248.

[46] M. Vasilopoulou, A.M. Douvas, D.G. Georgiadou, L.C. Palilis, S. Kennou, L. Sygellou, A. Soulatis, I. Kostis, G. Papadimitropoulos, D. Davatzoglou, P. Argitis, The influence of hydrogenation and oxygen vacancies on molybdenum oxides work function and gap states for application in organic optoelectronics, *J. Am. Chem. Soc.* 134 (2012) 16178–16187.

[47] B. Wang, Z. Hu, S. Liu, M. Jiang, Y. Yao, Z. Li, X. Ma, Effect of sulphidation temperature on the performance of NiO-MoO₃/γ-Al₂O₃ catalysts for sulphur-resistant methanation, *RSC Adv.* 4 (2014) 56174–56182.

[48] B. Liu, L. France, C. Wu, Z. Jiang, V.L. Kuznetsov, H.A. Al-Megren, M. Al-Kinany, S. A. Aldrees, T. Xiao, P.P. Edwards, Methanol-to-hydrocarbons conversion over MoO₃/H-ZSM-5 catalysts prepared via lower temperature calcination: a route to tailor the distribution and evolution of promoter Mo species, and their corresponding catalytic properties, *Chem. Sci.* 6 (2015) 5152–5163.

[49] Y. Li, F.-M. Li, X.-Y. Meng, S.-N. Li, J.-H. Zeng, Y. Chen, Ultrathin Co₃O₄ nanosheets for the oxygen evolution reaction, *ACS Catal.* 8 (2018) 1913–1920.

[50] P. Wang, H. Zhou, C. Meng, Z. Wang, K. Akhtar, A. Yuan, Cyanometallic framework-derived hierarchical Co₃O₄-NiO/graphene foam as high-performance binder-free electrodes for supercapacitors, *Chem. Eng. J.* 369 (2019) 57–63.

[51] X.T. Wang, T. Ouyang, L. Wang, J.H. Zhong, T. Ma, Z.Q. Liu, Redox-inert Fe³⁺ ions in octahedral sites of Co-Fe spinel oxides with enhanced oxygen catalytic activity for rechargeable zinc-air batteries, *Angew. Chem. Int. Ed.* 58 (2019) 13291–13296.

[52] X.Z. Liu, T. Tang, W.J. Jiang, Q.H. Zhang, L. Gu, J.S. Hu, Fe-doped Co₃O₄ polycrystalline nanosheets as a binder-free bifunctional cathode for robust and efficient zinc-air batteries, *Chem. Commun.* 56 (2020) 5374–5377.

[53] T. Ouyang, X.T. Wang, X.Q. Mai, A.N. Chen, Z.Y. Tang, Z.Q. Liu, Coupling magnetic single-crystal Co₂Mo₃O₈ with ultrathin nitrogen-rich carbon layer for oxygen evolution reaction, *Angew. Chem. Int. Ed.* 59 (2020) 11948–11957.

[54] X. Zhang, Y. Chen, M. Chen, B. Yu, B. Wang, X. Wang, W. Zhang, D. Yang, MOF derived multi-metal oxides anchored on N-doped carbon matrix as efficient and durable electrocatalyst for oxygen evolution reaction, *J. Colloid Interface Sci.* 581 (2021) 608–618.

[55] J. Li, Z. Xiong, Y. Sun, F. Li, Y. Feng, J. Liao, H. Li, M. Wu, H. Nan, K. Shi, Q. Liu, Balanced capture and catalytic ability toward polysulfides by designing MoO₂-Co₂Mo₃O₈ heterostructures for lithium-sulfur batteries, *Nanoscale* 13 (2021) 15689–15698.

[56] M. Li, Y. Wang, H. Yang, P.K. Chu, Hierarchical CoMoO₄@Co₃O₄ nanocomposites on an ordered macro-porous electrode plate as a multi-dimensional electrode in high-performance supercapacitors, *J. Mater. Chem. A* 5 (2017) 17312–17324.

[57] X. Li, L. Xiao, L. Zhou, Q. Xu, J. Weng, J. Xu, B. Liu, Adaptive bifunctional electrocatalyst of amorphous coke oxide @ 2D black phosphorus for overall water splitting, *Angew. Chem. Int. Ed.* 59 (2020) 21106–21113.

[58] K. Chu, Y.-H. Cheng, Q.-Q. Li, Y.-P. Liu, Y. Tian, Fe-doping induced morphological changes, oxygen vacancies and Ce³⁺-Ce³⁺ pairs in CeO₂ for promoting electrocatalytic nitrogen fixation, *J. Mater. Chem. A* 8 (2020) 5865–5873.

[59] Y. Dou, C.T. He, L. Zhang, H. Yin, M. Al-Mamun, J. Ma, H. Zhao, Approaching the activity limit of CoSe₂ for oxygen evolution via Fe doping and Co vacancy, *Nat. Commun.* 11 (2020) 1664.

[60] Y. Shi, J. Li, B. Zhang, S. Lv, T. Wang, X. Liu, Tuning electronic structure of CoNi LDHs via surface Fe doping for achieving effective oxygen evolution reaction, *Appl. Surf. Sci.* 565 (2021), 150506.

[61] L. Yu, Q. Zhu, S. Song, B. McElhenny, D. Wang, C. Wu, Z. Qin, J. Bao, Y. Yu, S. Chen, Z. Ren, Non-noble metal-nitride based electrocatalysts for high-performance alkaline seawater electrolysis, *Nat. Commun.* 10 (2019) 5106.

[62] D. Liu, H. Ai, J. Li, M. Fang, M. Chen, D. Liu, X. Du, P. Zhou, F. Li, K.H. Lo, Y. Tang, S. Chen, L. Wang, G. Xing, H. Pan, Surface reconstruction and phase transition on vanadium-cobalt-iron trimetal nitrides to form active oxyhydroxide for enhanced electrocatalytic water oxidation, *Adv. Energy Mater.* 10 (2020), 2002464.

[63] W. Liu, L. Yu, R. Yin, X. Xu, J. Feng, X. Jiang, D. Zheng, X. Gao, X. Gao, W. Que, P. Ruan, F. Wu, W. Shi, X. Cao, Non-3d metal modulation of a 2D Ni-Co

heterostructure array as multifunctional electrocatalyst for portable overall water splitting, *Small* 16 (2020), 1906775.

[64] Z. Liu, H. Liu, X. Gu, L. Feng, Oxygen evolution reaction efficiently catalyzed by a quasi-single-crystalline cobalt fluoride, *Chem. Eng. J.* 397 (2020), 125500.

[65] H. Tran Huu, W.B. Im, Facile green synthesis of pseudocapacitance-contributed ultrahigh capacity $\text{Fe}_2(\text{MoO}_4)_3$ as an anode for lithium-ion batteries, *ACS Appl. Mater. Inter.* 12 (2020) 35152–35163.

[66] J. Li, Y. Wang, H. Gao, S. Song, B. Lu, X. Tian, S. Zhou, Y. Yuan, J. Zang, Nickel boride/boron carbide particles embedded in boron-doped phenolic resin-derived carbon coating on nickel foam for oxygen evolution catalysis in water and seawater splitting, *ChemSusChem* 14 (2021) 5499–5507.